Adaptive Finite Element Simulation of Sheet Forming Operations Using Continuum Elements

Mohd. Ahmed
Civil Engineering Department
King Khalid University
Gregar, Abha-61411
KSA
moahmedkku@gmail.com

Abstract: - Presented in this study is the recovery techniques based adaptive finite element analysis of sheet forming operations. An adaptive finite element code **AdSheet2** considering continuum elements has been developed. The code allows the analysis of sheet forming operations and gives the distribution of adaptively refined mesh, effective strain, and punch load, stress and strain rate tensor in the domain. The recovery scheme for determining more accurate velocity field is based on the least squares fitting of the computed velocities in element patches. The solution error is estimated on the basis of an energy norm. The code is used to simulate an axi-symmetric stretching of a metal blank by a hemispherical punch. The numerical results of the adaptive analysis are presented and compared with non-adaptive analysis. The results presented show that the performance of the adaptive analysis in predicting the deformation behaviour i.e. the seats of large deformations, instability and effect of contact conditions is much superior.

Key-Words: - Stress Recovery, Velocity Recovery, Adaptive Mesh Refinement, Sheet Forming Operations, Finite Element Analysis, Error Estimators

1 Introduction

The finite element method is an effective tool for simulating metal forming processes. However, the accuracy of finite element results depends upon the approximation of the mathematical model, manner of domain discretization, choice of scheme for solution of system equations and method employed for computing derivatives of the state variable. Significant errors can creep in the computed solution unless special care is taken. Moreover, in metal forming processes, material undergoes large deformation and some of the elements may suffer severe distortion. This could also lead to inaccuracies in the computed results. The reliability of the simulation can be enhanced through error estimation and adaptive mesh refinement. The enough advances are made in the field of finite element error estimators and adaptive mesh refinement techniques. Among the different types of error estimators, the post processing or recovery type of error estimators [1] are perhaps most popular. Most recovery techniques are based on the least square fitting of velocity (or the displacement) field or their derivatives (stress field) by a higher order polynomial over an elemental or nodal patch. Zienkiewicz et al. [2] discussed error estimation procedures based on recovery techniques and their effectiveness in linear problems. They also discussed the super convergent patch recovery (SPR) technique and an alternative so-called recovery-by-equilibrium-in-patches (REP) technique. A recovery technique to extract derivatives and stresses based upon the least squares fitting of velocity field over an element patch has been presented by Singh et al. [3]. The optimization study of adaptive mesh refinement during finite element simulation of sheet forming operations has been carried out by Ahmed et al. [4]. Selmen et al. [5] has predicted wrinkling in Sheet Metal Forming using error indicators. The errors estimation procedure adopted by them is based on proposed combination of element thickness and geometrical error. An adaptive numerical analysis for deep drawing process has been carried out by Cherouat et al. [6]. An adaptive refinement procedure for metal forming process with ductile damage is presented by Giraud et al. [7] for 3D adaptive simulation and by Labergère [8] for 2D adaptive simulation. Ahmed and Singh [9] carried out the adaptive parametric study on Mesh Refinement during Adaptive Finite Element Simulation of Sheet Forming Operations. Chung et al. [10] has presented 3D- Finite element analysis of sheet metal forming process employing solid element remeshing procedures and effect of single and double layer of mesh on deformed shape and thickness variation of cold sheet forming process is studied.

Discretization of a sheet metal blank can be done on the basis of continuum elements or else by shell elements. Continuum elements discretize the sheet not only along its mid-surface but also across it i.e. along the direction of its thickness. Contact conditions are modelled independently on both sides of the metal blank. More than one layer of elements is used for considering variation of strains through the sheet thickness caused by bending and shear. Continuum elements were employed for analysis of sheet forming operation by Makinouch [11] using an elasto-plastic formulation, and by Oh and Kobayashi [12] using an elasto-plastic formulation and as well as using rigid-plastic analysis. The developments in the simulation of sheet metal forming using continuum elements have been presented by Ahmed, Sekhon, and Singh [13]. An extended version of the solid–shell finite element SHB8PS has been implemented into the implicit finite element code **ABAQUS** by Salahouelhadj et al. [14] and they applied it to sheet metal forming simulations. The aim of the present study is to compare the numerical results on axi-symmetric stretching of a metal blank using velocity recovery techniques and continuum element based adaptive procedures [3] with numerical results obtained from non-adaptive analysis.

2 Finite Element Formulation

During sheet forming operations, the material is subjected to larger strains. Hence the material is assumed to behave as a rigid plastic or rigid visco-plastic material. The flow formulation may be adopted to arrive at the finite element equations. It requires that among admissible velocities u_i that satisfies the conditions of compatibility and incompressibility, as well as the velocity boundary conditions, the actual solution gives the following functional (function of functions) a stationary value [11].

$$\pi = \int_{\Omega} \sigma'_{ij}\, \dot{\varepsilon}_{ij}\, d\Omega + \int_{\Gamma f} F_i\, u_i\, d\,\Gamma f \qquad (1)$$

$$\delta\pi = \int_{\Omega} \overline{\sigma}\, \delta\overline{\dot{\varepsilon}}_i\, d\Omega + K \int_{\Omega_v} \dot{\varepsilon}_v\, \delta\dot{\varepsilon}_v\, d\Omega - \int_{\Gamma f} F_i \delta u_i\, d\,\Gamma f \qquad (2)$$

where K is a large positive constant. Discretizing the domain and minimizing the functional gives the following relation.

$$\left[\frac{\partial \pi}{\partial V_i}\right]_{V=V_i} + \left[\frac{\partial^2 \pi}{\partial V_i\, \partial V_j}\right]_{V=V_0} \Delta V_j = 0 \qquad (3)$$

On simplifying the above, we obtain the following matrix equation

$$\boldsymbol{K}\ \Delta\boldsymbol{v}\ =\ \boldsymbol{f} \qquad (4)$$

where $\boldsymbol{K}$ is called the stiffness matrix and $\boldsymbol{f}$ is the residual of the nodal point force vector.

The boundary at time t can be assumed to be divided into three parts, namely S_1 on which velocity is prescribed, S_2, which is free and S_3 where frictional contact occurs. The following conditions apply on each type of boundary.

On S_1: $(v - v_o).\ \boldsymbol{n}\ =\ 0$ (5)

On S_2: $\boldsymbol{\sigma}\ .\ \boldsymbol{n}\ =\ 0$ (6)

On S_3: $\Delta v_t\ =\ (v - v_o).\boldsymbol{t}$ (7)

where v, v_o are the material and the die velocity, $\boldsymbol{n}$ & $\boldsymbol{t}$ are unit vectors in the normal and tangential directions with respect to the die surface, and $\boldsymbol{\sigma}$ is the stress tensor.

The magnitude of the frictional stress on the material is dependent on the magnitude of the relative sliding velocity u_s between the material and the die. Their directions of the frictional stress f_s and relative sliding velocity u_s are opposite to each other. Mathematically, the relationship between f_s and u_s may be expressed as follows.

$$f_s = -\, m\, k\, \frac{u_s}{\|u_0\|} \cong -\, m\, k\left(\frac{2}{\pi}\tan^{-1}\left[\frac{u_s}{u_0}\right]\right) \qquad (8)$$

where u_0 is a small threshold velocity, of the order of 10^{-3} to $10^{-4}\ u_s$.

A two-point reduced integration is employed for the penalty terms. The non-linear system equation is solved by Newton-Raphson algorithm. To achieve convergence linear line search technique has been used in the code.

3 Proposed Model

Fig. 1 shows a schematic of typical axi-symmetric sheet metal forming operation. The blank material is assumed as rigid-visco plastic or rigid-plastic. The elastic components of strain and strain rates are neglected as small. The punch and die are considered as rigid. The downward velocity of the punch can be arbitrarily specified. The flow rule for the blank material is given by the following Equation [15].

$$\dot{\varepsilon}_{ij} = \dot{\varepsilon}_{ij}^{NL} = \frac{1}{2\overline{G}}\left[\sigma_{ij} - \frac{\overline{v}}{1+\overline{v}}\sigma_{kk}\delta_{ij}\right] \qquad (9)$$

where $\bar{G} = \mu$ = non-linear viscosity of the material. The stress-strain relation of the material of the blank is as follows.

$$\bar{\sigma} = (1 + a\,\bar{\varepsilon})\,\dot{\bar{\varepsilon}}^{\,m} \qquad (10)$$

Quantitative assessment of the quality of the proposed model and adaptive mesh improvement to achieve target accuracy is carried out by simulating the sheet stretching operations. The recovery scheme for determining more accurate velocity field [3] is based on the least squares fitting of the computed velocities in elemental patches. The energy norm of the error is adopted for assessing of the quality of the solution and for adaptive mesh refinement. For adaptive mesh refinement, the error was equally distributed over the elements of the domain [16].

4 Illustrative Example

The two-dimensional computer code **Adsheet2** developed on the basis of the adaptive finite element procedures has been applied to the case of sheet stretching operation (Figure 1). Owing to symmetry, only one half of the blank was modelled. The input parameters were as follows.

Blank Material = Mild Steel
Sheet thickness h = 2mm
Clamping Radius of Blank (Rb) = 59.18mm
Radius Ratio (R_b / R_p) = 1.20
Velocity of Punch V = 1mm/sec
K (Mesh size reduction factor) =1.2
Target error = 8%

Stress-strain relation $\bar{\sigma} = 589\,(0.0001 + \bar{\varepsilon})^{\,0.216}$

where $\bar{\sigma}$ is effective stress and $\bar{\varepsilon}$ is effective strain

The displacement of punch was modelled in incremental steps. The displacement in each increment was limited such that it caused a maximum strain increment of 1% and the nominal duration of each increment was taken as 0.25sec. The domain was discretized using six noded triangular elements. For discussion purpose, the blank is divided into three regions. Region I is the portion between the centre of the blank and a point up to which the punch is in contact with the blank. Region II corresponds to the portion of the blank neither in contact with punch nor with the die or blank holder and region III refers to the portion of the blank, which is in contact with the die and the blank holder. The following paragraphs present the results using the non-adaptive and adaptive analysis.
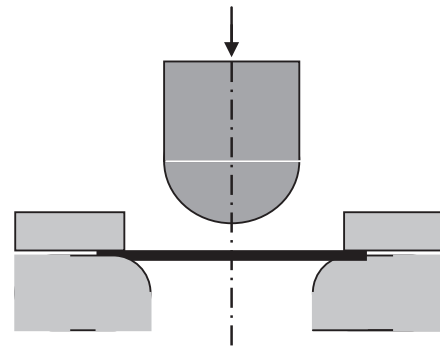

Fig. 1   Schematic Diagram of Sheet Stretching Operation

5 Adaptive Analyses

The adaptive analysis was carried out using velocity recovery techniques. A polynomial of degree 2 was taken for least squares fitting of the velocity since discretization of the domain had been carried out using quadratic elements. The fitting of velocity was done on a patch of elements surrounding the element under consideration while the fitting of stress was done on a patch of nodes surrounding the given node. The error was estimated in the energy norm. For adaptive mesh refinement, the error was equally distributed over the elements of the domain. The accuracy limit was taken as 8% of the global error. The computer memory requirement for storage of numerical result was about 150 MB. CPU time required for the analysis was approximately 7 hours. The average number of iterations per step required for convergence was 22. The average global error was 7.41%. Although the analysis provides detailed computational results for each time step, the results of only two stages of the deformation process are presented. Mesh and deformed shape and contours of components of strain tensor have been plotted at punch displacements of 2.5mm and 25.0mm.

5.1 Mesh Density

A user defined uniform mesh consisting of 828 elements and 3770 degrees of freedom was created at the beginning of the analysis (Figure 2). The computed solution was evaluated. As the error percentage in energy norm of the solution was more than the predefined error limit, the mesh was automatically regenerated. Two remeshings were required to bring the error below the predefined error limit. In the first remeshing, the number of elements and degrees of freedom were found to increase to 1239 and 5484 respectively. In the next remeshing, the number of elements and degrees of freedom decreased somewhat to 1031 and 4524

respectively. The global error of the solution after the second remeshing was found to be well below the prescribed limit in all subsequent steps. The element size reduces to approximately one fourth of the original size after remeshing in finer mesh zones. The computed mesh and deformed shapes at punch displacement of 2.5mm and 25.0mm are shown in Figure 3.

Referring to Figure 3 (a), which shows the deformed mesh at punch displacement of 2.5mm, it is observed that the region I and region III have finer elements. In region I, the maximum element density is at the punch-blank interface i.e. at the top surface of the sheet and it goes on decreasing towards the bottom of the sheet. The element density decreases along the radius too. The mesh in region II is more or less uniform but its density is smaller. The region III has a band of finer elements throughout its thickness.

The deformed mesh at punch travel of 25.0mm is given in Figure 3 (b). Though regions I and region III, continue to have greater number of fine elements but their distribution is significantly altered. Region I, which is localized at punch travel of 2.5 mm, becomes dispersed and the element density tends to decrease towards the region II. In region III also, two distinct bands of fine elements develop. The mesh in region II becomes coarser with increase of punch travel. As will become apparent from results presented later on, sites of highly dense elements correspond to seats of large deformation. In other words, the mesh refinement at a given location is proportional to the local gradients of velocity.
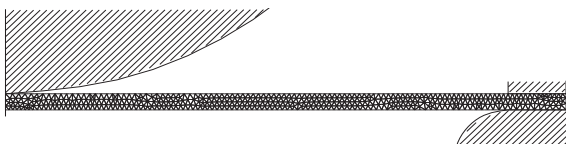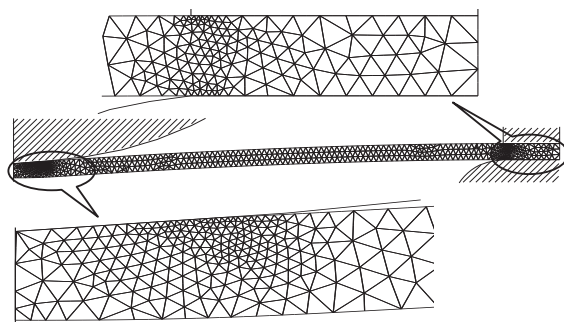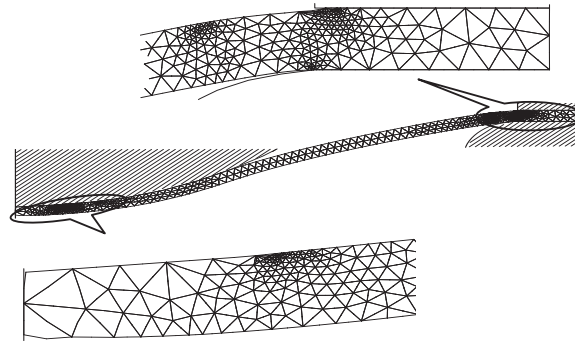

Fig. 2   Model and Initial Mesh

(a)   2.5 mm punch displacement

(b)   25.0 mm punch displacement

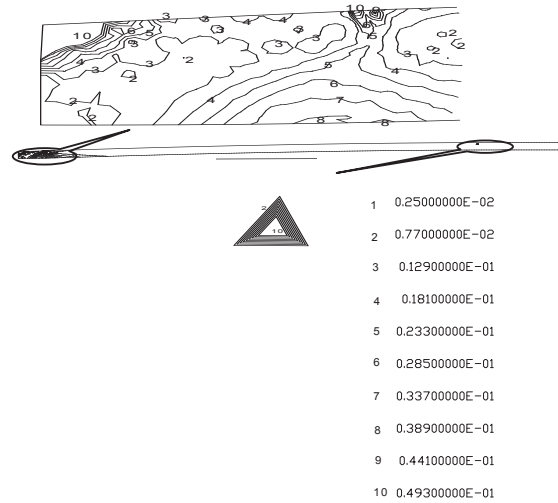Fig. 3   Deformed mesh using Adaptive Analysis

5.2 Effective Strain

Figure 4 shows the variation of effective strain at a punch displacement of 2.5 mm and 25.0 mm respectively. The magnitude of effective strain increases with increase of punch displacement. It is evident from the Figure 4 (a) that concentration of effective strain is predicted in two regions namely region I and region III. It is also observed that the maximum effective strain (equal to 0.0493) is predicted to occur at three locations, two in region I and one in region III. The location of maximum contour line is found near the top surface of blank. At the bottom of the sheet, maximum value contour has a value of 0.0389.
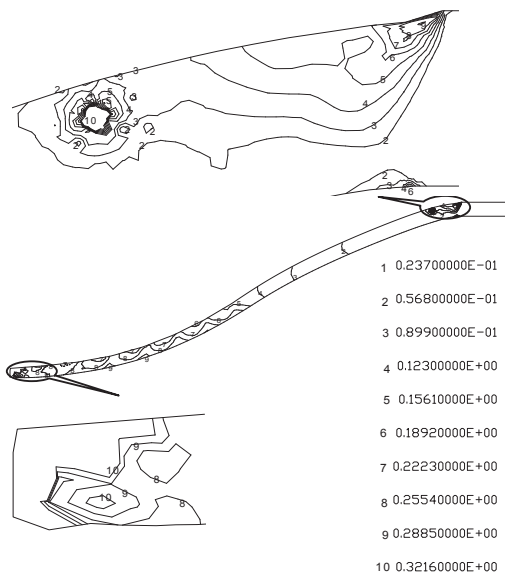
The distribution of effective strain at 25.0mm punch displacement is shown in Figure 4 (b). The magnitude of effective strain is found to increase in each region with increase of punch displacement. At locations around the centre of the blank, value of the effective strain is greater than 0.3216 across the sheet thickness. In region II, the effective strain varies from 0.0568 to 0.1561. In region III, two zones of high strain gradient are predicted. The bottom of the sheet in region III contains effective strain contour of maximum of value 0.1892. Contours of effective strain adjoining the top surface of sheet in region III, show that predicted effective strain is varies from 0.0237 to 0.3216.

The peak values and radial locations of effective strain at different punch displacements are listed in Tab. 1. The peaks increase in height with increase of punch displacement. Whereas the magnitude of the peak effective strain is 0.426031 at punch displacement of 2.5mm, it is as high as 3.016345 at 25.0mm of punch displacement. The radial location of the peak is also different at different punch displacement. Whilst the peak effective strain at 2.5mm and 25.0mm punch displacement is located

at the centre of the blank, it is located at the die corner radius during certain intermediate stages.

1	0.25000000E-02
2	0.77000000E-02
3	0.12900000E-01
4	0.18100000E-01
5	0.23300000E-01
6	0.28500000E-01
7	0.33700000E-01
8	0.38900000E-01
9	0.44100000E-01
10	0.49300000E-01

(a)   2.5 mm punch displacement

1	0.23700000E-01
2	0.56800000E-01
3	0.89900000E-01
4	0.12300000E+00
5	0.15610000E+00
6	0.18920000E+00
7	0.22230000E+00
8	0.25540000E+00
9	0.28850000E+00
10	0.32160000E+00

(b)   25 mm punch displacement

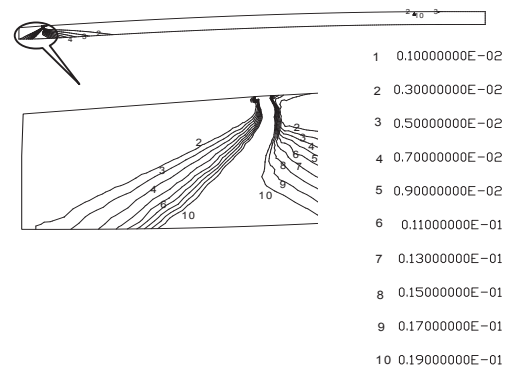Fig. 4 Contours of effective strain $\bar{\varepsilon}$ using Adaptive Analysis

Table 1: Peak $\bar{\varepsilon}$ and P Using Adaptive Analysis

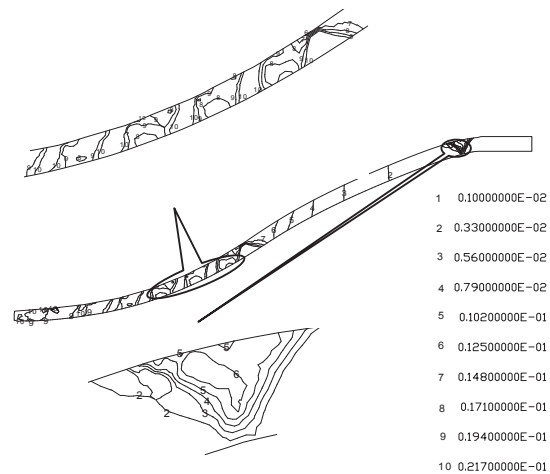| Punch travel (mm)	Effective Strain ($\bar{\varepsilon}$)	Location (mm)	Punch Load (P, kN)
2.5	0.426031	0.020	2.36
7.5	1.996043	55.80	12.96
12.5	2.001042	55.80	28.55
17.5	2.006001	55.70	47.78
25.0	3.016345	0.050	85.53

5.3 Effective Strain Rate

The distribution of effective strain rate at different values of punch displacement is depicted in Fig. 5 (a) and (b). It is found that there is only a marginal effect of punch displacement on the effective strain rate. It is observed from the Fig. 5 (a) that in region I, the maximum value contour (0.019/sec) extends throughout the sheet thickness. Region II has smallest values of the effective strain rate. In region III, highest value of the effective strain rate equals 0.19/sec.

From Fig. 5 (b), corresponding to punch displacement of 25.0mm, highest effective strain rate is found in region I. In region II, the value of the effective strain rate uniformly decreases towards the region III. The bottom of sheet, in region III, experiences lowest strain rate.

1	0.10000000E-02
2	0.30000000E-02
3	0.50000000E-02
4	0.70000000E-02
5	0.90000000E-02
6	0.11000000E-01
7	0.13000000E-01
8	0.15000000E-01
9	0.17000000E-01
10	0.19000000E-01

(a)   2.5 mm punch displacement

1	0.10000000E-02
2	0.33000000E-02
3	0.56000000E-02
4	0.79000000E-02
5	0.10200000E-01
6	0.12500000E-01
7	0.14800000E-01
8	0.17100000E-01
9	0.19400000E-01
10	0.21700000E-01

(b)   25 mm punch displacement

Fig. 5 Contours of effective strain rate $\dot{\bar{\varepsilon}}$ using Adaptive Analysis

5.4 Effective Stress

The contour plots of predicted values of effective stress corresponding to punch travel of 2.5mm and 25.0mm are given in Fig. 6. The values of effective stress increase with the increase of punch travel. Fig. 6 (a) containing contours of effective stress at a punch travel of 2.5mm indicates that stress concentration is pronounced in regions I and III, and the level of effective stress is higher than 174.0 N/mm2. In region I, the effective stress in the vicinity of the top surface varies from 234.0 to 270.0 N/mm2. Region II experiences more or less uniform level of effective stress. The predicted maximum magnitude of effective stress, in region III, is 270.0 N/mm2.

Fig. 6 (b) corresponds to punch displacement of 25.0mm. It shows two zones of stress concentration, one each in region II and III just near the junction. Region I experience a uniform effective stress of magnitude 430.0 N/mm2 except near the centre of the blank where highest level of stress occurs across the whole thickness of the blank.

When including a sub-subsection you must use, for its heading, small letters, 11pt, left justified, bold, Times New Roman as here.
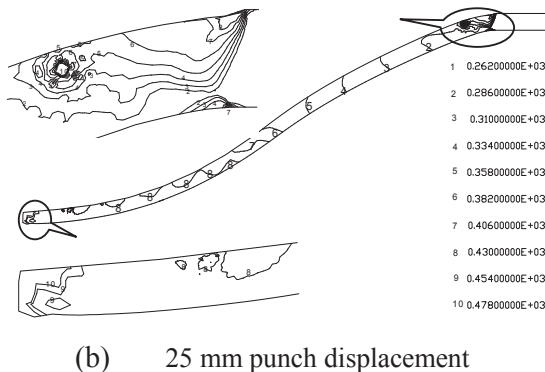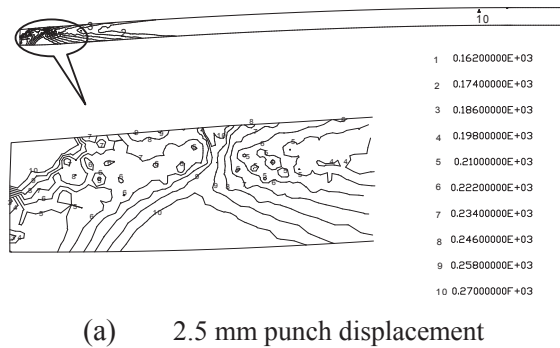
5.5 Components of Strain Rate Tensor

The predicted iso-value plots of components of strain rate are shown in Fig. (7) through (10).

Predicted variations of radial strain rate component $\dot{\varepsilon}_r$ at punch displacement of 2.5mm are shown in Fig. 7 (a). It is found that largest values of this component (both tensile and compressive) occur in regions I and III. In region I, it varies from 0.01 /sec (compressive) at the top surface to 0.0197 /sec (tensile) at the bottom surface. In region II, $\dot{\varepsilon}_r$ varies from 0.0001(compressive) to 0.00320(tensile). The variation in region III is from 0.0001 /sec (compressive) at the bottom surface to 0.0197 /sec (tensile) at the top surface. Fig. 7 (b) pertains to contours at punch displacement of 25.0mm. The nature of distribution is more or less similar in different regions of the sheet. The contours of highest magnitude appear in region I where the bottom surface experiences greater values of $\dot{\varepsilon}_r$ than the top surface. The variation in region II is from 0.00002/sec to 0.00178/sec. In region III, the tensile magnitude varies from 0.00002 /sec to 0.01058 /sec.
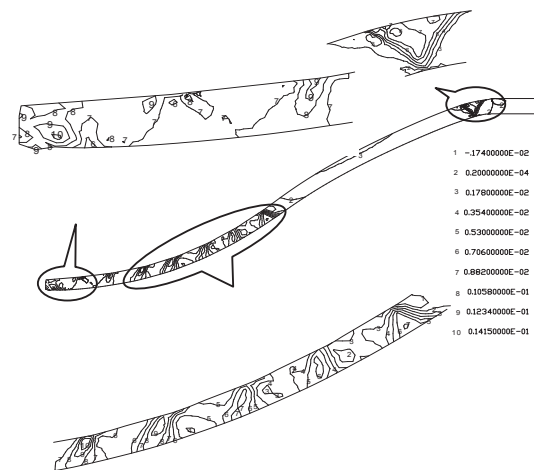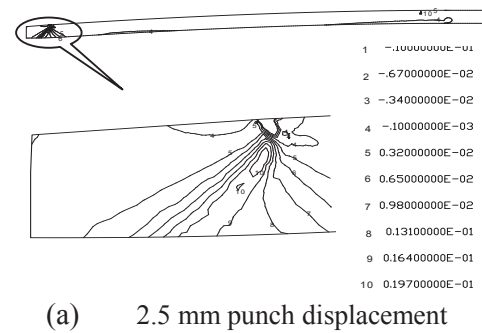

1	0.16200000E+03
2	0.17400000E+03
3	0.18600000E+03
4	0.19800000E+03
5	0.21000000E+03
6	0.22200000E+03
7	0.23400000E+03
8	0.24600000E+03
9	0.25800000E+03
10	0.27000000E+03

(a)   2.5 mm punch displacement

1	0.26200000E+03
2	0.28600000E+03
3	0.31000000E+03
4	0.33400000E+03
5	0.35800000E+03
6	0.38200000E+03
7	0.40600000E+03
8	0.43000000E+03
9	0.45400000E+03
10	0.47800000E+03

(b)   25 mm punch displacement

Fig. 6   Contours of effective stress $\overline{\sigma}$ using Adaptive Analysis

1	−.10000000E−01
2	−.67000000E−02
3	−.34000000E−02
4	−.10000000E−03
5	0.32000000E−02
6	0.65000000E−02
7	0.98000000E−02
8	0.13100000E−01
9	0.16400000E−01
10	0.19700000E−01

(a)   2.5 mm punch displacement

1	−.17400000E−02
2	0.20000000E−04
3	0.17800000E−02
4	0.35400000E−02
5	0.53000000E−02
6	0.70600000E−02
7	0.88200000E−02
8	0.10580000E−01
9	0.12340000E−01
10	0.14150000E−01

Fig. 7   Contours of strain rate component $\dot{\varepsilon}_r$ using Adaptive Analysis

The distribution of the axial strain rate component $\dot{\varepsilon}_z$ at different values of punch displacement is shown in Fig. 8 (a) and (b). The Former figure shows that $\dot{\varepsilon}_z$ at the top surface of region I and bottom surface of region III are in tension. Region II is in compression and the variation is from 0.00017/sec to 0.0064/sec. It is clear from Fig. 8 (b) depicting variation of $\dot{\varepsilon}_z$ at punch displacement of 25.0 mm that nature of this strain component throughout the sheet thickness is compressive. Region I is subjected to higher values of $\dot{\varepsilon}_z$ as compared to regions II and III. The lowest value contour of strain component has a magnitude of 0.00678 /sec, which stays constant throughout region II. In region III, $\dot{\varepsilon}_z$ varies from 0.00678/sec to 0.01014/sec.
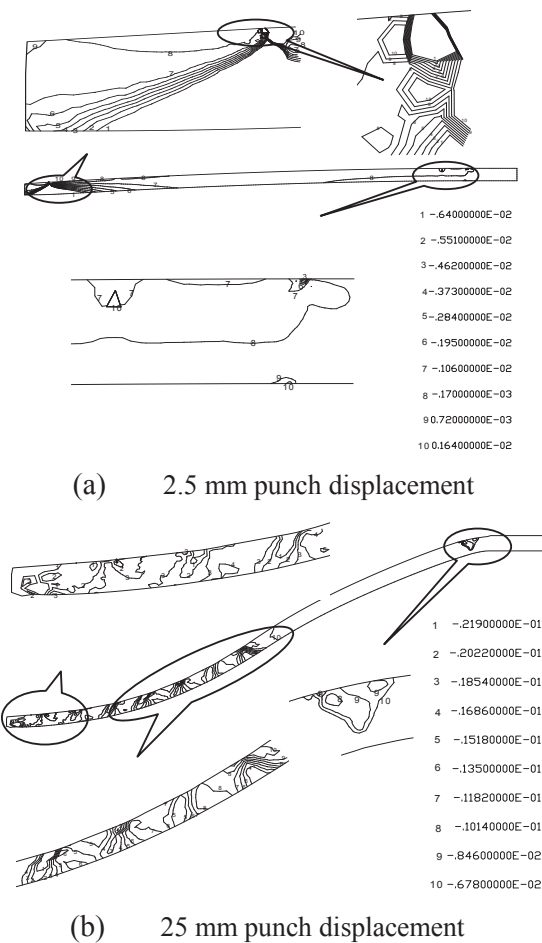

1	-.64000000E-02
2	-.55100000E-02
3	-.46200000E-02
4	-.37300000E-02
5	-.28400000E-02
6	-.19500000E-02
7	-.10600000E-02
8	-.17000000E-03
9	0.72000000E-03
10	0.16400000E-02

(a)   2.5 mm punch displacement

1	-.21900000E-01
2	-.20220000E-01
3	-.18540000E-01
4	-.16860000E-01
5	-.15180000E-01
6	-.13500000E-01
7	-.11820000E-01
8	-.10140000E-01
9	-.84600000E-02
10	-.67800000E-02

(b)   25 mm punch displacement

Fig. 8   Contours of strain rate component $\dot{\varepsilon}_z$ using Adaptive Analysis

The contour plots of the rate of hoop strain $\dot{\varepsilon}_\theta$ at 2.5mm and 25.0mm punch displacements are shown in Fig. 9. At a punch travel of 2.5m, highest magnitude of $\dot{\varepsilon}_\theta$ in region I is predicted to be 0.02002/sec. Region II has more or less a constant magnitude of $\dot{\varepsilon}_\theta$ throughout the region. The analysis predicts a compressive nature of this strain component at the interface between the blank holder and the sheet. The contours of $\dot{\varepsilon}_\theta$ at punch displacement of 25.0mm, given in Fig. 9 (b) indicate that in region I, compressive $\dot{\varepsilon}_\theta$ occur at the bottom surface and tensile $\dot{\varepsilon}_\theta$ develops at the top surface. The distribution of compressive $\dot{\varepsilon}_\theta$, in region II, varies from 0.00615/sec to 0.01716/sec. The variation of $\dot{\varepsilon}_\theta$ in region III is 0.00486/sec (compressive) to 0.00982/sec (tensile).

1	-.50000000E-02
2	-.25000000E-02
3	0.56000000E-03
4	0.33400000E-02
5	0.61200000E-02
6	0.89000000E-02
7	0.11680000E-01
8	0.14460000E-01
9	0.17240000E-01
10	0.20020000E-01

(a)   2.5 mm punch displacement

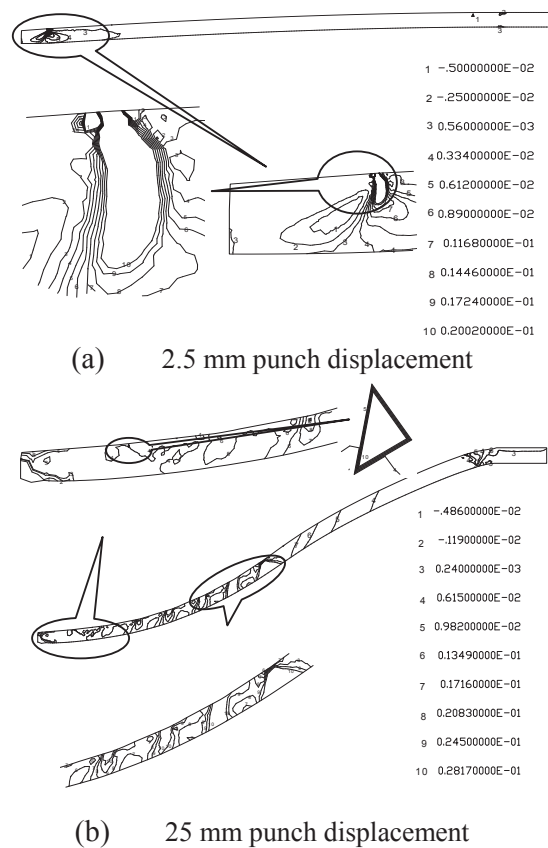|	
1	-.48600000E-02
2	-.11900000E-02
3	0.24000000E-03
4	0.61500000E-02
5	0.98200000E-02
6	0.13490000E-01
7	0.17160000E-01
8	0.20830000E-01
9	0.24500000E-01
10	0.28170000E-01

(b)   25 mm punch displacement

Fig. 9   Contours of strain rate component $\dot{\varepsilon}_\theta$ using Adaptive Analysis

Fig. 10 (a) and (b) depict the variation of the shear strain rate component $\dot{\varepsilon}_{r\theta}$ at different stages of deformation. It is clear from the contour plots that at a punch displacement of 2.5mm, part of the top surface and entire bottom surface of sheet of region I and region II are positive. Shear strain rate $\dot{\varepsilon}_{r\theta}$ is positive throughout regions III. The contour plots

for punch displacement of 25.0mm given in Fig. 10 (b) indicate that $\dot{\varepsilon}_{r\theta}$ is positive throughout except near the centre of the blank in region I. It is also found that high gradient of strain rate $\dot{\varepsilon}_{r\theta}$ occurs in region I near the centre of blank. The strain component uniformly decreases in magnitude in region II from 0.00876/sec to 0.00022/sec towards region III.
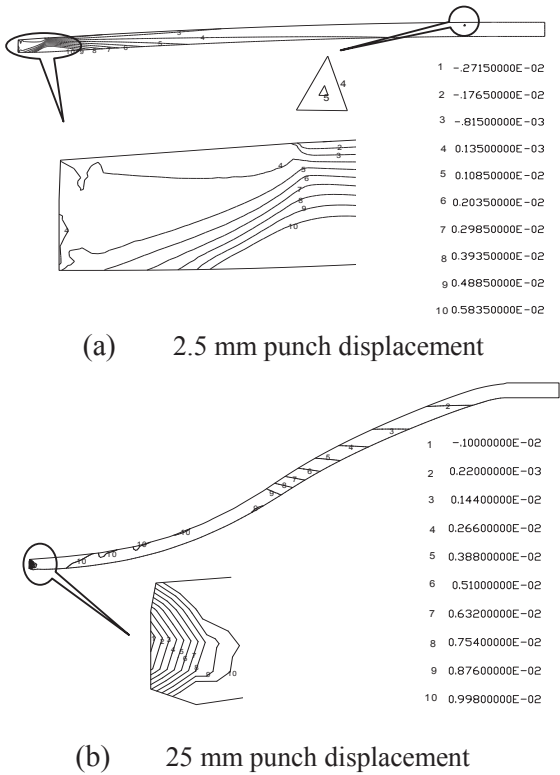

1	-.27150000E-02
2	-.17650000E-02
3	-.81500000E-03
4	0.13500000E-03
5	0.10850000E-02
6	0.20350000E-02
7	0.29850000E-02
8	0.39350000E-02
9	0.48850000E-02
10	0.58350000E-02

(a)   2.5 mm punch displacement

1	-.10000000E-02
2	0.22000000E-03
3	0.14400000E-02
4	0.26600000E-02
5	0.38800000E-02
6	0.51000000E-02
7	0.63200000E-02
8	0.75400000E-02
9	0.87600000E-02
10	0.99800000E-02

(b)   25 mm punch displacement

Fig. 10 Contours of strain rate component $\dot{\varepsilon}_{r\theta}$ using Adaptive Analysis

5.6 Punch Load
The punch load values at different stages of deformation are listed in the Table 1. It is evident from the table that punch load increases with increase of punch displacement. The predicted values of punch load at punch travel of 2.5mm and 25.0mm are 2.36 kN and 85.53 kN respectively.

6   Non-Adaptive Analysis
The computer memory requirement for storage of numerical result in case of non-adaptive analysis was 45 MB and CPU time was approximately 3.5 hours. The average number of iterations per step required for convergence was 27 and average global error was 9.75%. The mesh at punch displacement of 2.5mm and 25.0mm obtained from non-adaptive analysis is shown in Fig. 11. The user-defined mesh

consisted of 828 elements and 3770 degrees of freedom and remains unaltered throughout the blank at different stages of deformation.
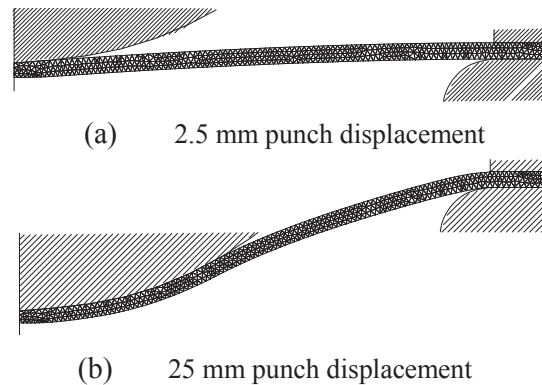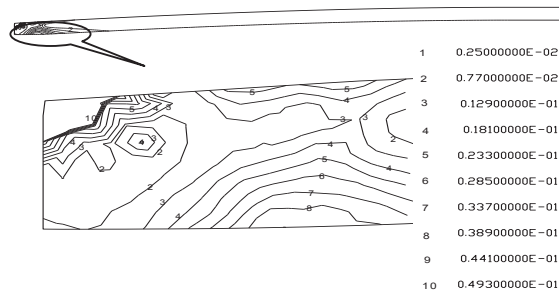

(a)   2.5 mm punch displacement

(b)   25 mm punch displacement

Fig. 11 Deformed mesh using Non-adaptive Analysis
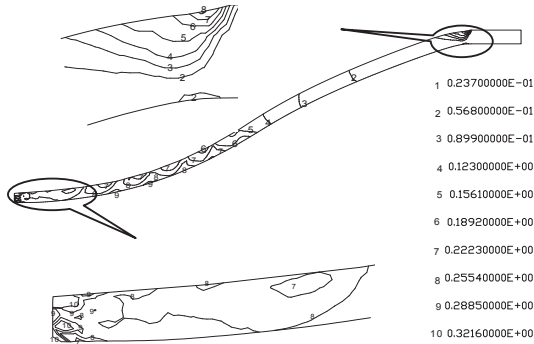
6.1 Effective Strain
Fig. 12 shows the variation of effective strain at punch displacement of 2.5mm and 25.0mm for non-adaptive analysis. The magnitude of effective strain increases with the increase of punch displacement. It is evident from the Fig.12 (a) giving effective strain at punch displacement of 2.5mm that only region one has strain concentration with non-adaptive analysis. The location of maximum contour line is near the top surface of blank. At bottom of the sheet, maximum value of contour is 0.0389.

The distribution of effective strain at 25.0mm punch displacement is shown in Fig. 12(b). The magnitude of effective strain was found increased in each region with increase of punch displacement. In the region one, at the centre of blank, the effective strain is more than 0.3216. In the second region, the effective strain varies from 0.0568 to 0.1560. In region three, one zone is showing high stress gradient. The highest value contour of effective strain, in region three at the bottom of sheet, was predicted to be 0.0568. The top surface of sheet, in region three, shows the contours magnitude variation from 0.0237 to 0.2554.

Table 2 a list the peak values and locations of effective strain at different stages of deformation predicted by non-adaptive analysis. The magnitude of the peak effective strain is 0.4260024 at punch displacement of 2.5 mm, while it is 0.726245 at 25.0 mm of punch displacement. The peak effective strain is located at the centre of the blank throughout the punch displacement.
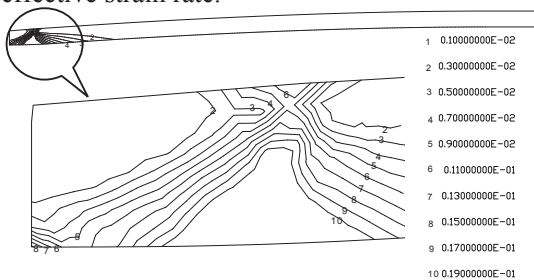
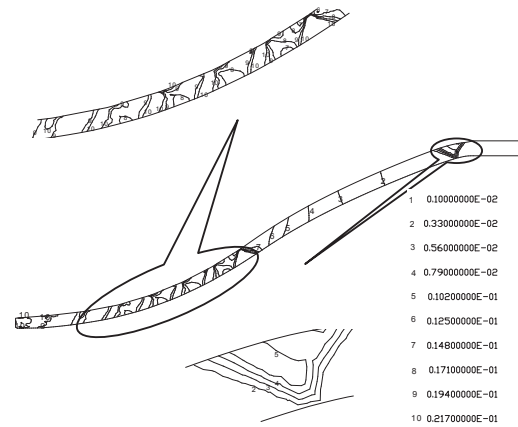(a)   2.5 mm punch displacement

(b)   25 mm punch displacement

Fig. 12 Contours of effective strain $\bar{\varepsilon}$
using Non-adaptive Analysis

6.2 Effective Strain Rate

The distribution of effective strain rate at 2.5mm and 25.0mm punch displacement are depicted in Fig. 13. It is clear from the Fig. 13(a) giving effective strain rate at punch displacement of 2.5mm that in region one, the maximum value contour i.e. 0.019 is not up to the full thickness of the sheet The region two has minimum value of effective strain rate. From Fig. 13(b), it is observed that variation of effective strain rate at punch displacement of 25.0mm is more or less similar in non-adaptive analysis. The region one has highest effective strain rate. In the region two, the value of effective strain rate uniformly decreased towards the region three. The bottom of sheet of region three has lowest value of effective strain rate.

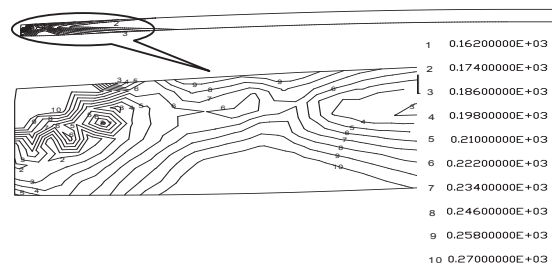(a)   2.5 mm punch displacement

(b)   25 mm punch displacement

Fig. 13 Contours of effective strain rate $\dot{\bar{\varepsilon}}$
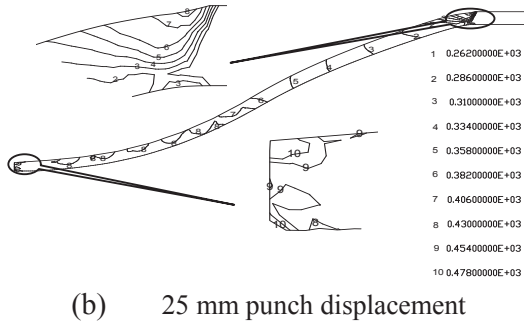using Non-adaptive Analysis

6.3 Effective Stress

The contour plots of effective stress are given in Fig. 14 at punch displacement of 2.5mm and 25.0mm for non-adaptive analysis. Fig. 14(a) showing contours of effective stress with non-adaptive analysis at punch displacement of 2.5mm indicate that only region one has stress concentration and effective stress more than 174.0 N/mm^2. In region one, the top surface of sheet has the magnitude of effective stress variation from 186.0 to 268.0 N/mm^2. Fig. 14(b) shows similar pattern of effective stress in region one and two at punch displacement of 25.0mm. In region three, the analysis predicts one zone of stress concentration.

6.4 Punch Load

Table 2 gives the magnitudes of punch load predicted by non-adaptive analyses at different stages of deformation. It is observed that the punch load in both the non-adaptive and adaptive analyses increases with increase of punch displacement. Also the predicted punch loads in case of either analysis were almost identical throughout the deformation process.

(a)   2.5 mm punch displacement

1	0.26200000E+03
2	0.28600000E+03
3	0.31000000E+03
4	0.33400000E+03
5	0.35800000E+03
6	0.38200000E+03
7	0.40600000E+03
8	0.43000000E+03
9	0.45400000E+03
10	0.47800000E+03

(b)   25 mm punch displacement

Fig. 14 Contours of effective Stress $\overline{\sigma}$
using Non-adaptive Analysis

Table 1: Peak $\overline{\varepsilon}$ and P using Adaptive Analysis

Punch travel (mm)	Effective Strain ($\overline{\varepsilon}$)	Location (mm)	Punch Load (P, kN)
2.5	0.426024	0.020	2.32
7.5	0.439744	0.019	12.83
12.5	0.488780	0.018	28.57
17.5	0.566371	0.015	47.91
25.0	0.726245	0.005	83.71

7 Discussion

During the course of the present work, a finite element code **AdSheet2**, was developed and the validation of the developed code is given in the published literature [9]. The results of simulation carried out with the help of the proposed computer code are discussed below.

An initial uniform mesh becomes non-uniform after automatic regeneration. The non-uniformity of mesh is different at different stages of deformation. The accuracy of an adaptive analysis is higher as compared to the non-adaptive analysis. However, the CPU time for adaptive analysis is greater as compared to that for non-adaptive analysis. The average global error in non-adaptive and adaptive analysis in the sheet stretching case was 10.13% and 7.41% respectively. The CPU time for non-adaptive and adaptive analysis was 3.5 hours and 7 hours respectively. Strain (and stress) gradients are greatly or in a smaller measure suppressed or dissipated by non-adaptive analysis, especially one employing uniform mesh density. At the initial stage of deformation in adaptive analysis, the strain concentrations are predicted at surfaces of the blank that are in contact with punch as well as with die. During the later stage of deformation, two zones of strain concentration are predicted near the die radius. The magnitudes of effective strain obtained from both analyses increase with increase of punch

displacement. Also the peak values of effective strain predicted by adaptive analysis were higher than those predicted by non-adaptive analysis. In the example case, the maximum values of effective strain is less than 1.0 at punch travel of 25.0mm in non-adaptive analysis while values in excess of 3 are predicted by the adaptive analysis at this stage of deformation. The difference in the values of effective strain at early stages of deformation was more as compared to during the later stages of deformation. A difference of 353.9% was found at a punch travel of 2.5mm, which decreased to 254.8% at a punch travel of 25.0mm. The location of peaks at various stages of deformation predicted by non-adaptive analysis was near the centre of blank. However adaptive analysis predicted the locations of peaks differently. During the earlier stages of deformation, the locations were near the centre of blank, with increase of deformation, the peaks shifted outward to near the inner radius of the die. Later still, the peak again shifted to the centre of the blank.

The radial, axial and hoop strain rate components at early stage of deformation are higher in the portion of the sheet blank that is in contact with punch. Also high strain rate gradients are developed in this portion. During later stages of deformation, the radial, axial and hoop strain component appears to divide the sheet under the punch into bands of high and low magnitude of strain rates. These bands may be the zones of instability. The shear strain rate components at all stages of deformation is higher in the portion of the sheet blank that is in contact with punch and a high strain rate gradient is also developed in this portion. It is also found that there is no significant difference between punch loads predicted by the adaptive and non-adaptive analysis.

The variation of tool and blank contact effect in adaptive and non-adaptive environment is clearly observed. The mesh is refined at the contact regions. At large stress and strain gradients in region of contact, the uniform initial mesh is refined through the thickness when the blank is in contact on both faces while it is refined only on one face when tool is in the contact of one face of blank. At the outer edge of contact during initial stages of deformation, the various stress and strains in adaptive analysis show large gradient through the thickness, while with increase of deformation, stress and strains distributed to a larger extent. In non-adaptive analysis, there is no wide variation in stress and strains due to tool contact to blank at different stages of deformation.

The performance of the adaptive procedure appears to be good since it creates finer meshes in

regions of high strain (or stress gradient) on the side of the tool contact with the blank and the coarse meshes in regions of low strain (or stress gradient). The contours of maximum magnitude of effective strain, effective strain rate and effective stress are found to occur at more than one location with adaptive analysis but only at one location in non-adaptive analysis. Highest value of effective strain contours covers whole sheet thickness with adaptive analysis while it is in some portion of the sheet thickness with non- adaptive analysis. It can be infers from the above discussion that the adaptive analysis seems to exhibit a true picture of deformation behaviour and adaptive analysis may be usefully employed to predict the seats of large deformations , locations of possible instability and effect of continuously changing tool contact conditions on the sheet forming operations.

4 Conclusion

In this study, two-dimensional computer code **Adsheet2** based on recovery based adaptive finite element procedures to simulate metal forming operation has been developed. A post-processing type of error estimator has been employed for finding elemental and global error. The recovery scheme for determining more accurate velocity field is based on the least squares fitting of the computed velocities in elemental patches. Significant conclusions of the study are summarized below.

- The prediction of the two-dimensional code **AdSheet2** showed good agreement with results available in the published literature.
- Results of simulations of adaptive analysis show that the mesh becomes finer only in regions of high strain gradients and it become coarser in regions of low strain gradient. The seat of high strain gradients corresponds to tool- blank interfaces. The uniform initial mesh is refined through the thickness when the blank is in contact on both faces while it is refined only on one face when tool is in the contact of one face of blank. The mesh size reduces to approximately one fourth of the original size after remeshing in finer mesh zones.
- The comparison of adaptive analysis with non-adaptive analysis indicates that the adaptive analysis predicts higher values of effective strain as compared to the non- adaptive analysis. Also, the locations of peaks of effective strain are different at different stages of deformation. This is because strain gradients can get suppressed or dissipated in non-adaptive

analysis, especially one employing uniform mesh density.

- The variation of effective stress and strain predicted by two analyses is also different. The adaptively reduced mesh size show a true picture of state variables variation through the thickness. The non-adaptive analysis shows the maximum value of to a part of thickness while adaptive analysis predicted it to be throughout the thickness or up to a greater thickness.
- The study of components of the strain rate tensor during the axisymmetric sheet stretching operation predicted by the velocity recovery based analysis indicates that the radial, axial and hoop strain rate components at earlier stage of deformation is higher in the portion of the sheet blank that is in contact with punch. During later stages of deformation also, high radial, axial and hoop strain rate components are developed in the same portion of blank. But high strain rates also happen in the portion of the blank that is in contact with the die. The cumulative axial and hoop strain components at this stage, appears to divide the sheet under the punch into bands of high to low magnitude of strain rates. The shear strain rate components at all stages of deformation are higher in the portion of the sheet blank that is in contact with punch.

References:
[1] Zienkiewicz, O. C. and Zhu, J. Z., "A simple error estimator and adaptive procedure for practical engineering analysis", Int. J. Num. Meth. Engg.,Vol. 24, 1987, pp. 335-357.
[2] Zienkiewicz, O. C., Boroomand, B. and Zhu, J. Z., "Recovery Procedures in Error Estimation and Adaptivity, Part I, Adaptivity in Linear Problems", *Comm. App. Num. Meth.*, Vol. 176, 1999, pp. 111-125.
[3] Singh, D., Sekhon, G. S. and Shishodia, K. S., "Finite Element Analysis of Metal Forming Processes With Error Estimation and Adaptive Mesh Generation", *Proc. of 11th ISME Conf.*, 1999, pp. 616-621.
[4] Ahmed, M., Sekhon, G. S. and Singh, D., "Optimization of Adaptive Mesh Refinement During Finite Element Simulation of Sheet Forming Operations", *Proc. IMPLAST'03, 8Th International Symposium on Plasticity and Impact Mechanics*, Gupta, N.K., eds., Delhi, 2003, pp 1065-1074.
[5] Selman, A., Meinders**,** T., Boogaard van den, A.H. and Huétink, J., "Adaptive Numerical Analysis of Wrinkling in Sheet Metal

Forming", *International journal of forming processes*, 6 (1)., 2003, pp. 87-102.

[6] Cherouat, A., Giraud, M. L., Borouchaki, H., Adaptive Refinement procedure For Sheet metal Forming, *Proceedings 9th International Conference NUMIFORM '07*, AIP Conference Proceedings, Volume 908, 2007, pp. 937-942.

[7] Giraud, M. L., Borouchaki, H., Cherouat, A., "Adaptive remeshing for sheet metal forming in large plastic deformations with damage", *Int. J. Material Processing (suppl.)*, 1, 2008, pp. 129-132.

[8] Labergère, C., Rassineux, A. A., Saanouni K. K., "2D adaptive mesh methodology for the Simulation of Metal Forming Processes with Damage", *International Journal of Material Forming,* 4(3), 2011, pp. 317-328.

[9] Ahmed, M., Singh, D., An Adaptive Parametric Study on Mesh Refinement during Adaptive Finite Element Simulation of Sheet Forming Operations, Turkish J. Eng. Env. Sci., 32, 2008, 163-175.

[10] Chung, W., Kim, B., Lee, S., Ryu, H. and Joun, M. (2014), Finite element simulation of plate or sheet metal forming process using tetrahedron MINI-element, J. Mech. Science and Technology, 28 (1), 2014, pp. 237-243.

[11] Makinouchi, A., "Elastic-Plastic Stress Analysis of Bending an Hemming of Sheet Metal Forming Process", *Metallurgical Society Inc.,* N.M. Wang & S.C. Tang (eds.), 1985, pp. 161-176.\

[12] Oh, S. I. and Kobayashi, S. "Finite Element Analysis of Plane-strain Sheet Bending", Int. J. Mech. Sci., Vol. 22, 1980, pp. 583-594.

[13] Ahmed, M., Sekhon, G. S. and Singh, D. "Developments in The Finite Element Simulation of Sheet Metal Forming Processes", Defence Science journal, Vol. 55, No. 4, 2005, pp. 29-42.

[14] Salahouelhadj, A., Abed-Meraim F., Chalal, H. and T. Balan, (2012) "Application of the continuum shell finite element SHB8PS to sheet forming simulation using an extended large strain anisotropic elastic–plastic formulation", Archive of Appl. Mech., Vol. 82, 9, 2012, pp 1269-1290.

[15] Honer, M. E.; Wood, R. D., Finite Element Analysis of Axisymmetric Deep Drawing Using A Simple Two-Noded Mindlin in Shell Element. *Numerical Methods for Non-linear Problems*, Pinridge Press, 1987, pp. 440-449.

[16] Li, X. D. and Wiberg, N. E., "A Posteriori Error Estimate by Element Patch Post-processing, Adaptive Analysis in energy and L^2 Norms", Comp. Struct., 53, 4, 1994, pp. 907-919.